Chapter 2 Background

This chapter illustrates the background of PMR relevant to the discussions and results in the thesis. Section 2.1 introduces the basic principles of perpendicular recording and characteristics of magnetic properties. Section 2.2 describes different perpendicular magnetic recording layer and one kind of recording layers is the main research of this thesis. Section 2.3 is a collective conclusion of the decisive factors of recording performance for R&W test.

2.1 Principles of Perpendicular Recording

2.1.1 Introduction

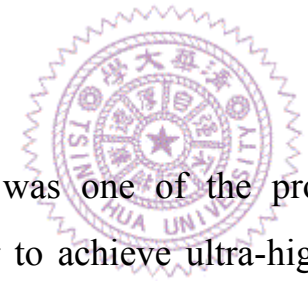

The previous H.D.D. was one of the products of the longitudinal magnetic media. In order to achieve ultra-high density of the recording media, the size of magnetic cluster has to be shrunk with concerns of low noise media. However, the magneto-crystalline anisotropic energy of the longitudinal magnetic media is failed to resist the thermal fluctuation of room temperature. It is likely to cause the thermal instability and subsequently limit the lifetime of the recording bits. Although the latest invention of the AFC media [2] had extended the development of longitudinal recording media, perpendicular recording media is no doubt the best candidate for the recording density beyond 100 Gb/in^2.

2.1.2 Basic Concepts of Perpendicular Recording

In 1975, S. Iwasaki [3] proposed the modern ideas of the perpendicular recording media that the magnetizations are perpendicular to the film but not parallel the film. Figure 2.1 illustrates the magnetic moment directions of the two kinds of these thin film media.

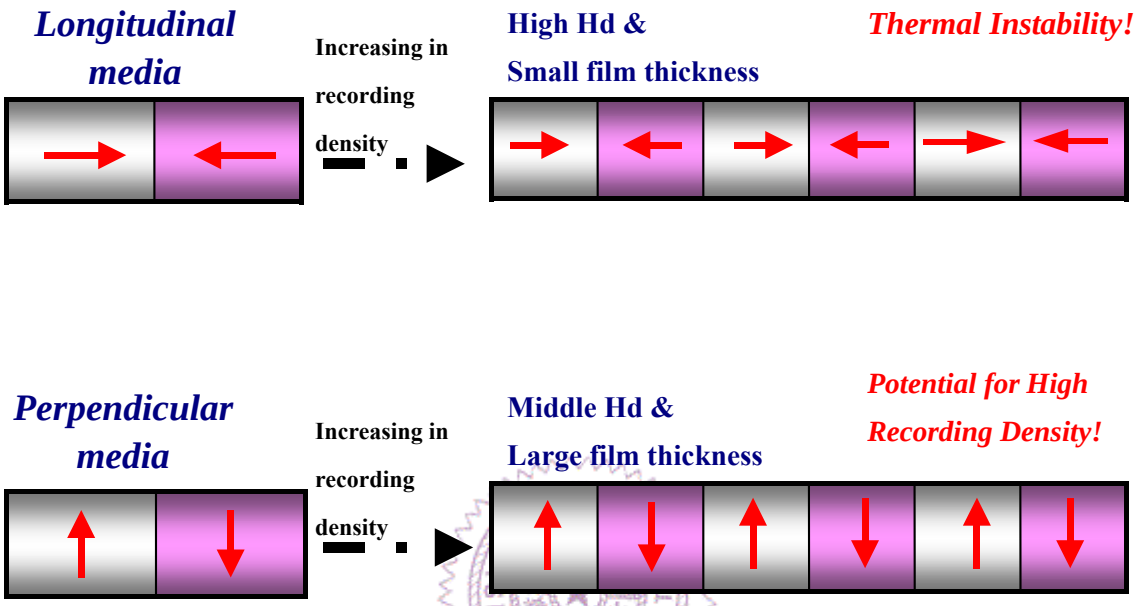

Figure 2.1 The configurations for longitudinal media and perpendicular media.

Due to the shape effect of the magnetic moments, large demagnetization field (H_d) would occur on the longitudinal recording media, which results in serious thermal instability. On the other hand, the demagnetization field of the perpendicular media is much smaller than that of the longitudinal one due to its shape of magnetic domain. As a consequence, perpendicular recording media is most suitable option for promoting the recording density to ultrahigh grade.

2.1.3 Perpendicular Anisotropy and Thermal stability

There are alternative terms of magnetic energy which would determine

the perpendicular anisotropy. One of these is magnetostatic energy resulted from free poles and external field. In addition, it depends on the shape of an object and demagnetization (H_d). For the perpendicular recording, the magnetization is physically normal to the film. Fig. 2.2 shows the relation between magnetization and demagnetization of the perpendicular thin film.

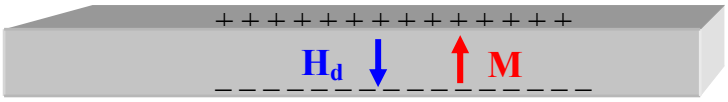

Figure 2.2 Effect of demagnetization field on perpendicular thin film media.

Since the demagnetization of the perpendicular thin film is $4\pi M_s$, the magnetostatic energy would be $0.5H_dM_s=2\pi M_s^2$. In order to overcome the effect of demagnetization, we have to choose the material of high magnetocrystalline anisotropy such as CoPtCr-SiO_2, FePt, and $[Co/Pd]_n$ as the magnetic recording layer. Indicating that the energy of magneto-crystalline anisotropy $\boldsymbol{K_u}$ is required to be lager than $2\pi M_s^2$. Fig. 2.3 shows H_k versus $4\pi M_s$ for different kind of perpendicular media where anisotropy field H_k is defined as $2\boldsymbol{K_u}/M_s$ [4].

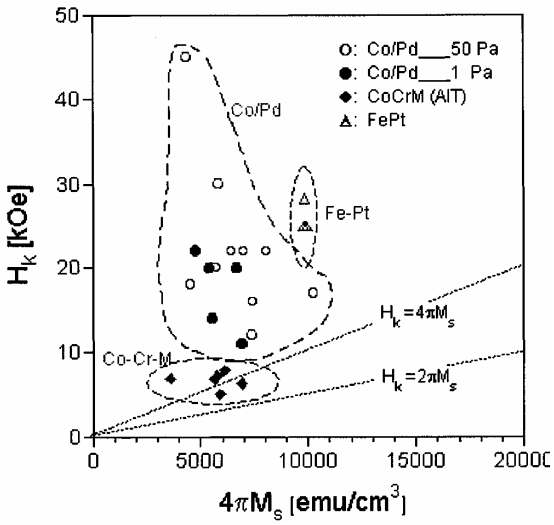

Figure 2.3 Comparisons of the anisotropy field of various recording materials. [4]

The perpendicular anisotropy is a vital factor of thermal stability which is defined as $K_u V/k_B T$, where V is the magnetic switching volume. Enhancement of thermal stability is essential for the sake of considering the supermagnetic effect as increasing the recording density. It is interpreting that the anisotropic energy becomes more and more important while reducing the magnetic grains and magnetic cluster size. In general, the value of $K_u V/k_B T$ is required to be larger than 60 in order to keep thermal stability of the media [5].

2.1.4 Magnetic Properties of PMR

In addition to perpendicular anisotropy, large perpendicular coercivity (Hc), unity squreness(SQ=Mr/Ms), a loop slope parameter(α value) near 1, and large negative nucleation field (Hn) are also decisive factors of magnetic properties. The larger coercivity represents the most potential for the ultrahigh recording media for the reason of resisting the thermal fluctuation and the demagnetization. Fig. 2.4 plots the Hc versus $4\pi M_s$ for perpendicular media [4].

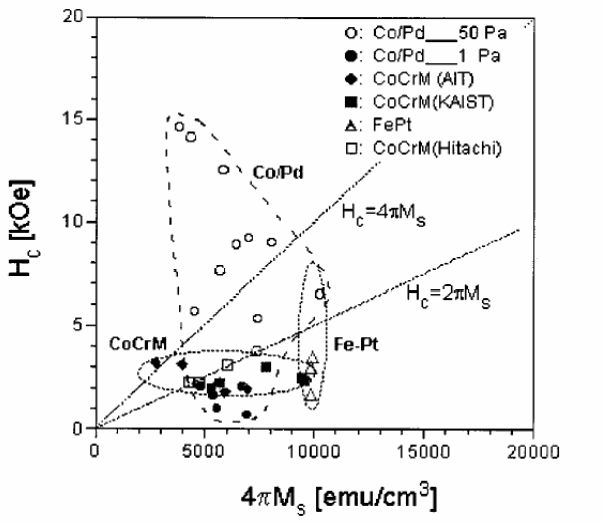

Figure 2.4 Hc versus 4πMs plot for various perpendicular recording media [4].

The media with the magnetic properties of SQ=1 and α=1 should have a perpendicular coercivity (Hc) greater than 4πMs. Large SQ is also preferable for maintaining thermal stability of residual magnetization of perpendicular recording media. Furthermore, negative nucleation field (Hn) is defined as a field of intersection for a saturation magnetization level and a slope tangent at Hc in hysteresis loop as shown in Fig. 2.5. As we have seen, higher Hc is also relatively required to obtain a large negative Hn.

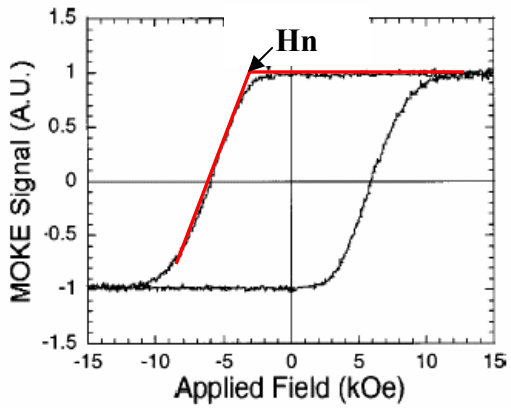

Figure 2.5 The position of nucleation field in a M-H loop[15].

2.1.5 Basic Recording Mechanism of PMR [6]

Unlike the recording ring head of longitudinal media, perpendicular media adopt a special head named “single-pole head (SPT head)” as shown in Fig. 2.6. In writing process, the main pole shoots magnetic flux across the recording layer and then come back to auxiliary pole through soft underlayer; therefore, the magnetic flux would be completely closed with no loss. In particular, this process is able to reduce demagnetization effectively. Moreover, the single-pole head/ soft underlayer configuration can provide approximation twice the field a longitudinal ring head does.

For various advantages, this modern design is in favor of ultrahigh-density perpendicular media.

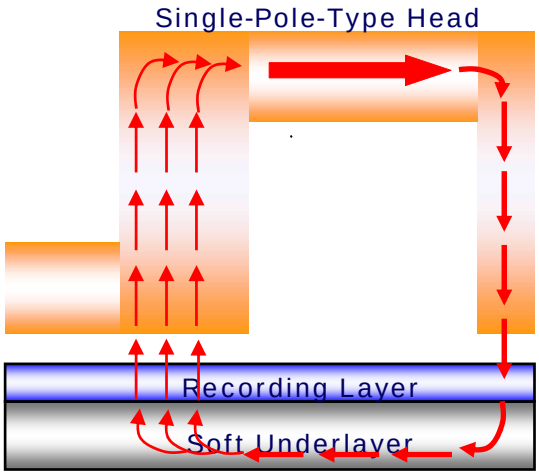

Figure 2.6 Scheme of perpendicular recording.

2.1.6 Requirements of high density PMR [4] [6]

1. ***High coercivity*** is needed in order to obtain small and sharp transition. However, the coercivity of media should not exceed the writing field of the head.
2. ***High remnant magnetization, Mr at small thickness δ of recording layer*** will contribute to readback signal which is proportional to Mr δ. It should be large, in the meantime, minimize the spacing loss of thickness.
3. ***Maintaining thermal stability*** for the sake of the fluctuation from thermal disturbance, it is essential to recording magnetization.
4. ***Uniform, small and isolated magnetic grains*** lead inter-granular coupling decreased as well as the noise.

2.2 Magnetic Recording Layer (RL)

Film Structure of PMR

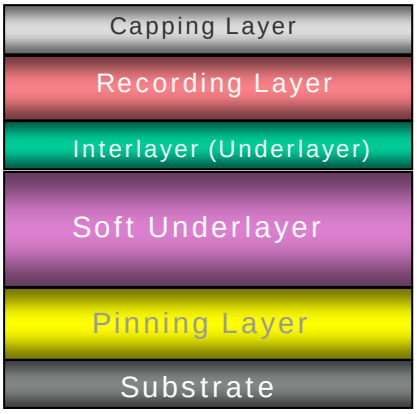

Figure 2.7 Whole structure of full-stacked perpendicular media.

The whole structure of full-stacked perpendicular media is shown in Fig. 2.7. As we have seen, the soft underlayer and pinning layer are included with granular system.

HSING HUA UNIVERSITY

- **Intermediate Layer (Underlayers)**

For perpendicular recording, the magnetic properties can not simply obtain by depositing single magnetic recording layer. In order to enhance the texture of c-axis orientation which is normal to the film, the intermediate layers are inserted for controlling the epitaxial growth of the upper magnetic layer. In general, the materials with HCP structure and with little mismatch lattice compared to the recording layer are inclined to be adopted as the candidates for underlayers. In addition, improving perpendicular anisotropy and reducing grain size of recording layer are also the benefits of inserting proper underlayers.

- **Soft Underlayer and Pinning Layer [7]**

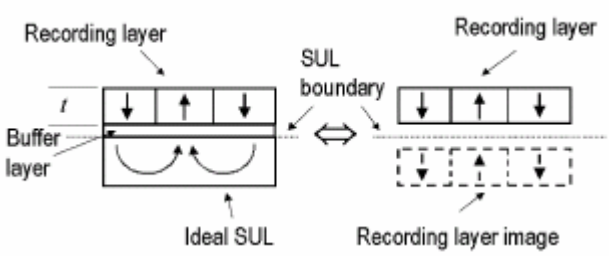

Figure 2.8 An illustration of the mirror-imaging by an ideal SUL.[7]

In 2002, D. Litvinov proposed that an ideal SUL as described in Fig. 2.8 is equivalent to the perfect mirror-imaging of the recording layer with respect to the SUL boundary. If there is no buffer-layer between recording layer and SUL, a two-fold increase of recording layer thickness would present by an ideal SUL. Furthermore, the pinning layer is introduced to reduce domain walls in SUL due to additional spike noise by F/AF and soft magnetic/hard magnetic exchange coupling. Through the combination of SUL/pinning layer, the performance of SNR is consequently enhanced.

Introduction

Perpendicular recording media are broadly studied such as CoCr-based, FePt, and $[Co/Pd]_n$ or $[Co/Pt]_n$ multilayer. The comparisons of these novel technologies are shown in Table 2.1.CoCrPt is the most promising candidate for perpendicular recording for it has been widely studied in longitudinal media. Since the storage research centers of H.D.D. industry could save the budget for new instruments, they could merely change the structure of the magnetic film for ultrahigh density. In this thesis, we will

emphasize on the recording layer of granular CoPtCr-SiO_2 and the discussion of parameter study of each layer of granular system.

Table 2.1 Comparisons of different perpendicular media.

	Advantages	Disadvantages
CoCr-based	♦ Suitable for the recent recording mechanism	♦ Lower Ku and Hc than others ♦ Segregation and thermal stability needed to be improved
FePt	♦ High Ku and Hc ♦ High Ms ♦ Potential of future development	♦ High ordering temperature of process ♦ Large grain size about 40nm ♦ High exchange coupling ♦ Large demagnetization
$[Co/Pd]_n$ $[Co/Pt]_n$	♦ Higher Ku and Hc ♦ Potential of future development	♦ Difficult process for multilayer ♦ Large grain size and bad SNR

2.2.1 CoCrPt media

There are several conclusive discussions of CoCrPt perpendicular recording media. For examples, changing the composition of CoCrPt, adding fourth elements into CoCrPt media, introducing proper underlayers, enhancing Cr segregation at grain boundaries, and reducing the stacking faults or fcc-like regions are the most familiar issues. We will interpret these five parts as following.

Changing the composition of CoCrPt

In general, magnetic properties attribute to Co element which is hard magnetic material and take the highest proportion of magnetic grains. On the other hand, Cr element plays an important role of separating grains isolated and Cr mainly contributes to the magnetic properties and the perpendicular anisotropy. However, Pt element is adopted for enhancing the perpendicular anisotropy ***Ku***. The larger ***Ku*** value is increased as increasing the proportion of Pt element; however, the exchange coupling and the grain size are also increased. T. Keitoku, *et al.* had researched in terms of the composition and the relationships between compositions and coercivity [8]. Figure 2.9 shows their results of compositional diagram and perpendicular Hc. It is indicating that the enhancement of perpendicular Hc was obtained in the proportion of Cr element and Pt element about 13 – 18 at% and 12 – 22 at%, respectively.

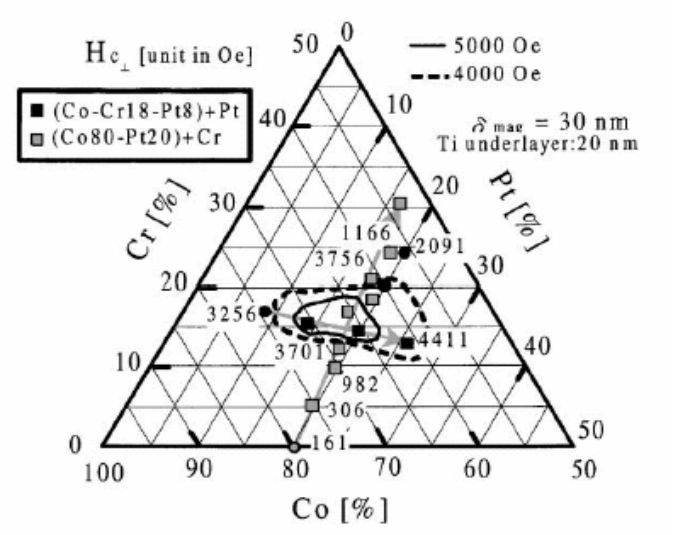

Figure 2.9 Hc⊥ in compositional diagram of CoCrPt ternary alloy films with 30nm thickness on Ti under-layer.[8]

Adding fourth elements into CoCrPt media

Adding the forth element into the CoCrPt such as Ta and Nb can both refine grain size and reduce the inter-granular exchange coupling. Although CoCrPtB and CoCrPtTa media have better performance of SNR than CoCrPt media, the thermal stability and perpendicular coercivity of CoCrPtB and CoCrPtTa are both sacrificed instead by the adding.

Introducing proper underlayers

In order to obtain highly [0002] texture of c-axis which is aligned perpendicular to the film, we introduce the proper underlayers between the recording layer and soft underlayer. In general, we choose the underlayer with HCP structure for the reason of little lattice mismatch such as Ru, Ti, and CoCr. In addition, we could also choose the amorphous underlayers such as Ti and Ta for diminishing the roughness of the film and offering a specific surface energy that could enhance the c-axis texture effectively. Table 2.2 illustrates the storage performance of perpendicular media with different underlayers.

Enhancement of Cr segregation by post-annealing

In addition to these techniques, it can be improved by enhancing the Cr segregation. For example, post-annealing is a valid and effective method to isolate the grains. We could improve the segregation by introducing a diffusion layer below or above the recording layer. In last year, S. Saito, *et al*. reported that newest Ti-CoCrPt-Ti media showed remarkable improvement of Hc up to 9.1 kOe by post-annealing process as shown in

Fig.2.10 [9]. It is one of the best and impressing results of CoCrPt media by post-annealing. However, the grain size of the recording layer by post-annealing is likely to be larger than the one without post-annealing and subsequently deteriorates the recording performance of SNR.

Table 2.2 Achievement of every corporation in perpendicular media.

Film Structure	**Performances**	**Institution**
$CoZr_{45}$/ Ti/ $CoCr_{16.9}Pt_{10.8}$ [10]	Hc~3.5 kOe, S~1, Ku~2.1*10^6 erg/cm^3	KAIST (1999)
Ta/ Ru/ $CoCr_{18}Pt_{16}B_4$	Hc~3.5 kOe, S~1, $H_K > 10$ kOe	MMC
C/Ti/CoCr/$CoCr_{19}Pt_8B_4$ [11]	Hc~3.5Koe, S~0.88	Tohoku University (2002)
NiFeMo/ Ta/ Ru/ $CoCr_{18}Pt_{16}B_4$ [12]	Hc~3.4 kOe, S~1	MMC(2002)
Ta/ $CoCr_{16}Pt_8$	Ms~630 emu/cm^3, Hc~4.27 kOe, S~0.92	Tohoku University
$TiCr_{10}$/ $CoCr_{19}Pt_{10}$	Hc~4 kOe	Hitachi
NiP/Ti/ CoCrPt [13]	Hc~3.5 kOe, S~0.6	DSI of Singapore(2001)
$TiCr_{10}$/ $CoCr_{20}Pt_{10}$	Hc~3.5 kOe, grain size~14 nm	Fuji and Tohoku University
Ta/ Ru/ CoCrPt [14]	Hc~2.7 kOe, S~0.88	Seagate (2002)
SUL/ IL/ CoCrPt(B) [15]	Ms~520 emu/cm^3, Hc~5.5 kOe, Hn~-500 Oe,	Seagate (2003)
Ag/Ti/$(Co_{78}Cr_{22})_{86}Pt_{14}$ [16]	Hc~3970Oe , Hn~2380Oe	Chongiu University and Samsung (2003)
C/Pt/$Co_{62}Cr_{16}Pt_{18}Nb_4$ [17]	Hc~3.7KOe, S~1	AIT (2003)
TiCr/MgO/$CoCr_{25}Ru_{25}$/$CoCr_{19}Pt_{10}$[18]	Hc>4.2KOe ,	Hitachi (2000)
CoTaZr/C/CoCr/$CoCr_{16}Pt_{15}Ta_3$ [19]	Hc~3233Oe, S~0.937	Hitachi (2002)
NiAl/Ti/$CoCr_{20}Pt_{10}$ [20]	Hc~5000 Oe , grain sizes~8.2nm	IBM (2001)

	materials of layer		non-annealed		annealed	
	under-layer	cap-layer	H_c (kOe)	S	H_c (kOe)	S
A	Ti	-	4.0	1.0	6.7	1.0
B	Ta	-	3.9	1.0	3.0	1.0
C	Pt	-	3.4	0.8	1.6	0.8
D	Ru/Ti	-	4.3	0.8	3.4	0.8
E	Ti	$Mn_{50}Si_{50}$	4.0	1.0	6.9	0.8
F		Ru	4.0	1.0	7.4	1.0
G		$Cr_{50}Mn_{50}$	4.0	1.0	7.9	1.0
H		Ti	4.0	1.0	9.1	1.0

Figure 2.10 Hc and SQ for nonannealed and annealed media with stacking structure of cap-CoCrPt-under.[9]

Reducing the stacking faults or fcc-like regions [21] [22]

For perpendicular media, the lattice match is always good between the underlayer [e.g., Ru (00.2)] and the magnetic layer, Co hcp-(00.2) or Co fcc-(111). Consequently, there is no available constraint that could limit the fcc growth and contributes to more fcc and SFs in the perpendicular media than in the longitudinal media, which is shown in Fig. 2.11 and Fig 2.12.

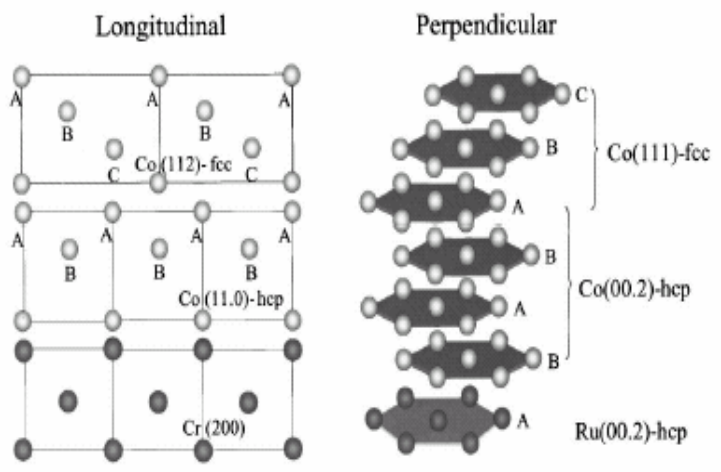

Figure 2.11 Schematic diagram of the epitaxial relationships in longitudinal (left) and perpendicular media (right).[21]

For improving the anisotropy of perpendicular magnetic media of Co-alloy grains, it is necessary to reduce the number of stacking faults (SFs) by controlling the crystal structure during the early stage of film growth.

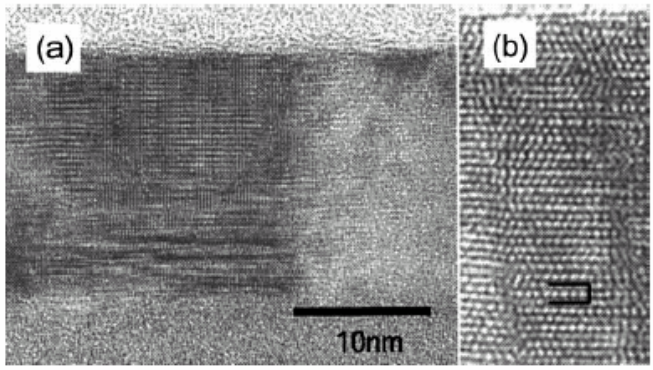

Fig. 2.12 Cross-sectional TEM images of a CoCrPt fabricated at 330 °C. (a) Overall image (b) Magnified lattice image of a portion in which the (11.0) plane can be observed. The mark indicates a SF.[22]

In particular, the stacking fault density increases as increasing the temperature of film fabrication as shown in Fig. 2.13. For instance, the density was 10% at a fabrication temperature of about 250 °C. In addition, the amount of SFs was large in the initial region of film growth due to interfacial stress with the underlayer. It is also found that an increase in SF density reduced Ku and the perpendicular Hc. Fig. 2.14 shows the relationship between the Ku and SF density.

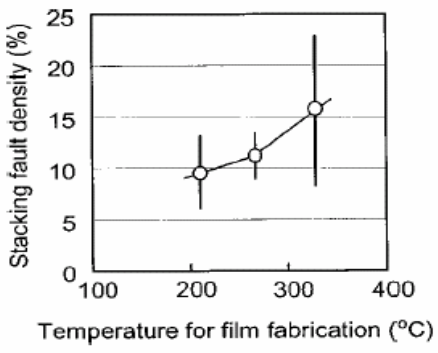

Figure 2.13 SF density as a function of temperature for magnetic film fabrication.[22]

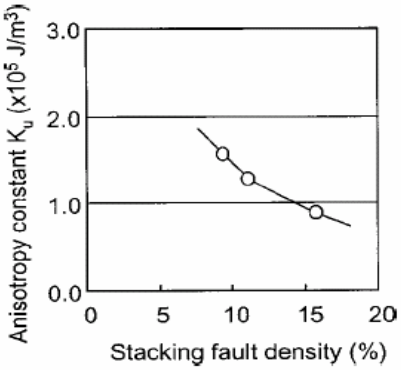

Figure 2.14 Anisotropy constant Ku vs SF density.[22]

Challenges of CoCrPt

Although many improvements of CoCrPt have been adopted, there still exist some trade-offs of larger grain size and achievement of SNR by thermal process. In addition, the mechanism of Cr segregation is not completely improved even though post-annealing at high temperature. Furthermore, Cr segregation is very difficult to achieve well-isolated grains because there are no sufficient high-angle grain boundaries to improve Cr segregation as CoCrPt longitudinal media. Moreover, there are no appropriate underlayers which could not only match the epitaxial growth perfectly of recording layer but also diminish the SF density effectively. In conclusion, there are several problems of CoCrPt media yet and the magnetic performance has limited by these constraints. All we need to do is to explore a new system which could solve the problems successfully and get even higher magnetic performance.

Recently, oxide granular media such as CoCrPtO or CoCrPt-SiO_2 have been proposed to provide better grain isolation via oxygen-rich grain boundaries without disturbing the epitaxial growth of CoCrPt. Further, oxide media show higher coercivity and negative nucleation fields. The granular media is one kind of composite thin film that consists of non-magnetic matrix and magnetic grains, i.e. the magnetic grains are surrounded by the non-magnetic materials. Well-isolated grains could reduce the inter-granular exchange coupling and therefore improve the SNR. Nowadays, many advanced storage groups have added this kind of oxide additives into magnetic layer to get well-isolated grains.

2.2.2 Granular CoCrPtO media [23]-[27]

By changing the oxygen to argon ratio (O_2/Ar ratio) during the deposition process, magnetic properties and magnetic loop shape can be validly controlled. The tendency of Hc increase with incremental oxygen gas ratio was observed in Fig. 2.15 and Fig. 2.16

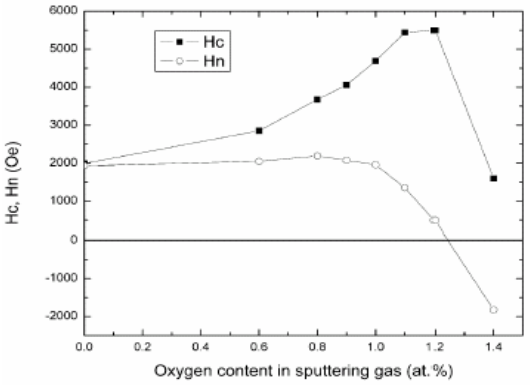

Figure 2.15 Hc and Hn dependence on oxygen gas ratio in the sputtering gas.[23]

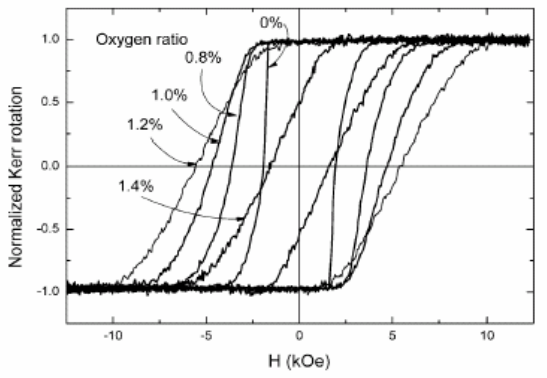

Figure 2.16 Kerr loops for the samples deposited with various oxygen ratios.[23]

For achieving good thermal stability of CoCrPtO media, it is necessary to reduce the grain size and its rather high media noise by improving grain uniformity and isolation. Obviously, the TEM image shown in Fig. 2.17 improves granular media and also presents more uniform grain morphology with clearly defined grain boundaries.

The magnetic performances of CoCrPtO are improved by increasing the thickness of Ru underlayer due to enhancement of c-axis orientation of recoding layer as shown in Table 2.3 and Figure 2.18. In addition, the average grain size is 7.2 nm with a standard deviation of 1.0 nm of CoCrPtO media with the 24nm Ru underlayer is shown in Fig. 2.19, which is the optimal reducing of magnetic grain size through oxide

materials segregation.

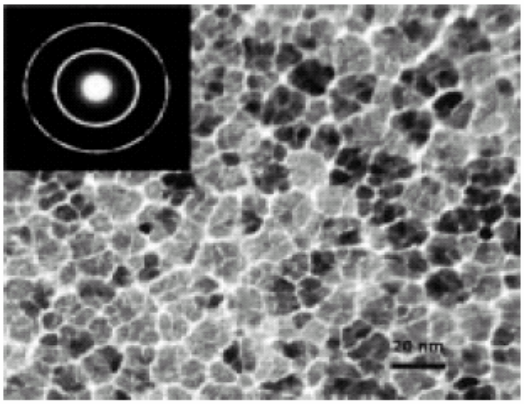

Figure 2.17 TEM image of the low noise CoCrPtO media. The electron diffraction pattern indicates a strong c axis out-of-plane alignment.[24]

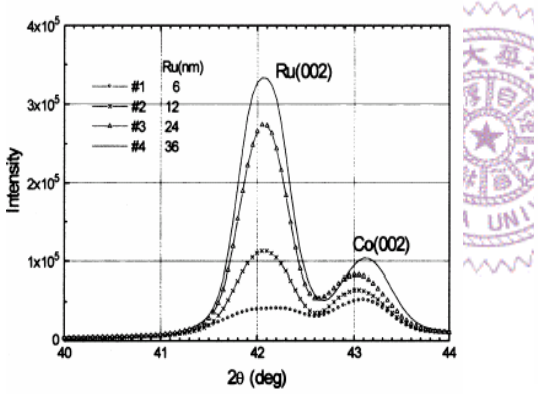

Figure 2.18 X-ray diffraction patterns of CoCrPtO media at varying Ru thickness [26].

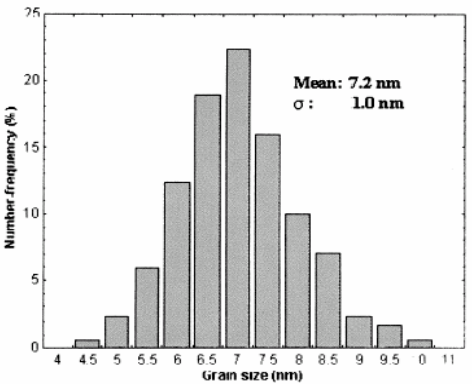

Figure 2.19 Grain size distributions of CoCrPtO media with 24nm Ru interlayer [26].

Ru (nm)	Half width [Rocking Curves] (degree)		H_c (Oe)	SNR (dB)	PW_{50} (nm)
	Ru (00.2)	Co (00.2)			
6	3.34	3.57	2947	5.5	95.8
12	2.86	3.10	4215	9.7	73.2
24	2.66	2.50	5284	11.6	74.6
36	2.52	2.39	5461	12.9	76.0

Table 2.3 Effects of Ru thickness of CoCrPtO media [26].

In particular, CoCrPtO layer on NiFeNb soft magnetic underlayer (SUL) showed higher Hc of 5000 Oe and well isolated grain in comparison with CoCrPtO layer on CoZrNb SUL. Different coercivity behaviors may be associated with residual stress as well as surface roughness induced with different SUL as indicated in Table 2.4.

Film structure (nm)	Residual Stress (MPa)
NiFeNb(200)	853
Ru(20)/Ta(5)/NiFeNb(200)	70
CoCrPtO(20)/Ru(20)/Ta(5)/NiFeNb(200)	480
CoZrNb(150)	-100
Ru(20)/Ta(5)/CoZrNb(150)	-450
CoCrPtO(20)/Ru(20)/Ta(5)/CoZrNb(150)	-311

Table 2.4 Residual stress induced on the films during the sputtering [25].

國立清華大學 NATIONAL TSING HUA UNIVERSITY

Compare CoCrPtO with CoCrPtB

From Table 2.5, we could find that oxide media have higher coercivity (>5000 Oe) than alloy media and achieve almost unity squareness, which may due to better grain segregations and fewer stacking faults. Better SNR and higher D_{50} have been obtained from oxide media and shown in Fig. 2.20 and Fig.2.21.

Media	H_c (Oe) H_n (Oe) SQ	SpSNR (dB)	Res. (%)	$OW_{67/17}$ (dB)	PW_{50} (μin.)	LF (mV)
CoCrPtB	2800 900 0.7	14.9	46	43.8	3.55	1.35
CoCrPtO	5100 -1500 1	14.9	68	44.5	3.1	1.22

Table 2.5 Parametric data for best alloy media and oxide media tested at 560 kfci.[27]

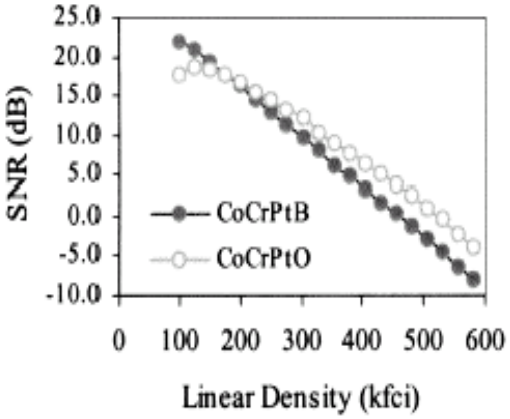

Figure 2.20 SNR versus linear density for CoCrPtO and CoCrPtB media [26].

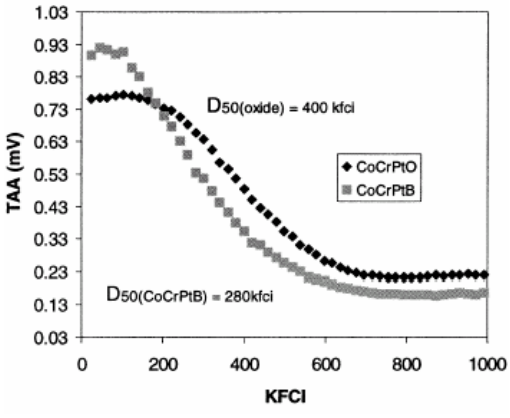

Figure 2.21 TAA as a function of linear density for CoCrPtB and CoCrPtO [27].

2.2.3 Granular CoPtCr-SiO_2 media

Optimization of SiO_2 Content [28]

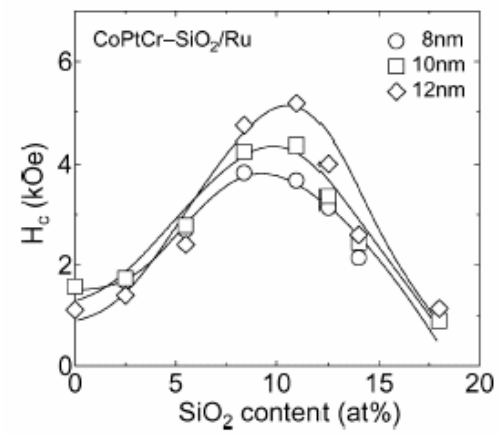

Figure 2.22 Values of Hc as a function of SiO_2 content with various film thicknesses [28].

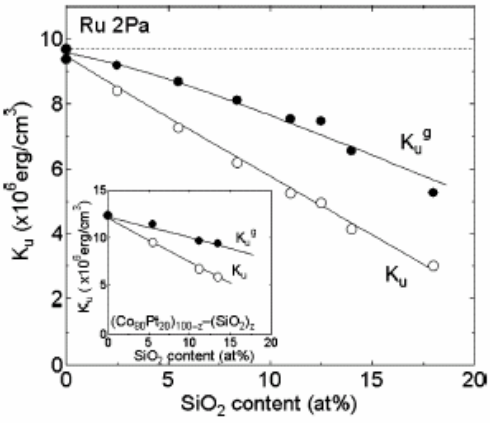

Fig 2.23 Value of ***Ku*** as a function of SiO_2 content [28].

In 2004, Y. Inaba indicated that the Hc increased significantly as the SiO_2 content of $\{(Co_{90}Cr_{10})_{80}\ Pt_{20}\}_{100-z}$-$(SiO_2)_z$ media increased and exhibited a maximum of Hc at about 11 at % SiO_2, i.e. 30 vol% SiO_2, as indicated in Fig. 2.22. These results imply that the addition of SiO_2 up to 11at % effectively enhances segregation and contribute to the

improvement of Hc. Conversely, the anisotropy ***Ku*** is obviously reduced while the SiO_2 content is increasing continuously as shown in Fig. 2.23, which is due to the reduction of Cr content in CoPtCr grains. It is indicating that a structural change of CoPtCr grains occurs as increasing the SiO_2 content.

However, the ***Ku*** of the CoPtCr-SiO_2 media exhibits a large value of $7*10^6$ erg/cm^3, even at 10 at % SiO_2 addition. There is no doubt that CoPtCr-SiO_2 media have a significant potential to resist thermal agitation of magnetization.

Fig. 2.24 shows TEM bright field image of 10nm CoPtCr-SiO_2 media with 11% SiO_2 contents. The D_{grain} including grain boundary thickness of SiO_2 decreases significantly from 8.8 to 5.4 nm as the SiO_2 content increases from 0 to 14.4 at % (～36 vol %). The hcp (002) lattice plane of the CoPtCr layer has a continuously epitaxial growth on the Ru (002) plane. The c-axis distribution $\Delta\theta_{50}$ of the CoPtCr grains is evaluated about 8^o by X-ray diffraction analysis.

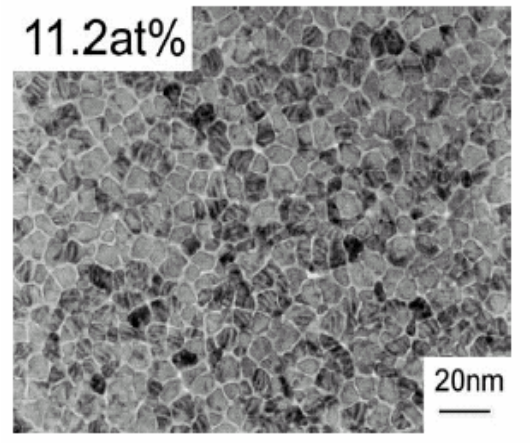

Figure 2.24 TEM image of 11.2 at% SiO_2 content of CoPtCr-SiO_2 media [28].

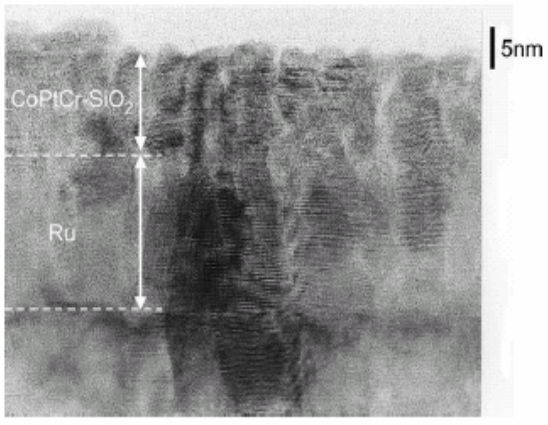

Figure 2.25 HR-TEM image of the cross section of CoPtCr-SiO_2 media [29].

CoPtCr-SiO_2/Ru Granular System [30]

The magnetic properties of CoPtCr-SiO_2 strongly depend on the sputtering condition of Ru intermediate layer such as thickness, sputtering pressure, and substrate temperature on the magnetic and microstructural properties. For example, the enhancement of the coercivity from 2.2 to 3.7 kOe is merely due to increase the sputtering pressure of Ru intermediate layer from 5 to 20 mTorr as shown in Fig. 2.26.

In addition, increasing the roughness of Ru underlayer is likely to enhance Hc, which is due to enlarge domain wall pinning. It is indicated in Fig. 2.27.

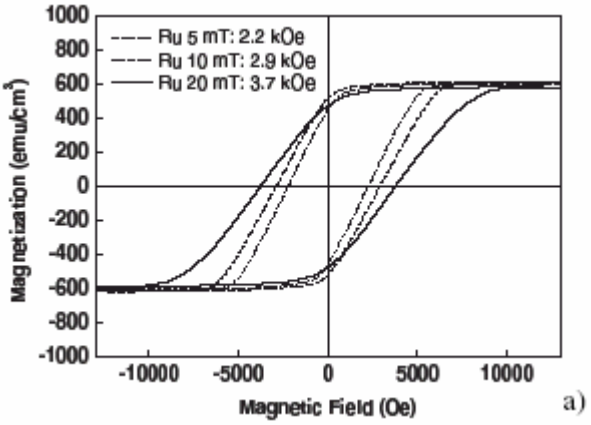

Figure 2.26 Dependence of perpendicular magnetic hysteresis curves for samples with Ru layers deposited at 5, 10, and 20 mTorr.[30]

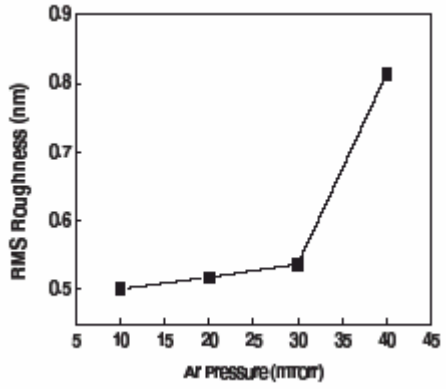

Figure 2.27 Surface morphologies of 30nm Ru films deposited at various sputtering pressures. Rootmean-square (RMS) roughness as a function of Ar pressure.[30]

Compare CoPtCr-SiO_2 with CoCrPtB [31]

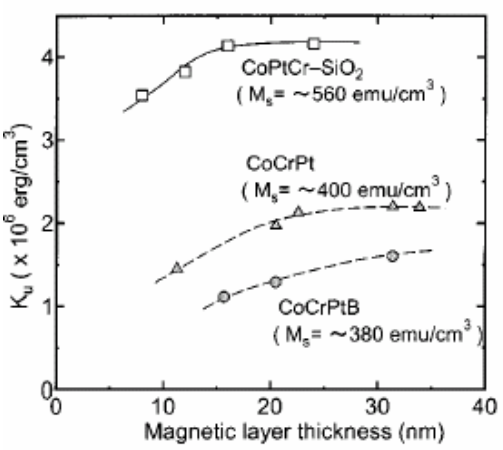

Figure 2.28 Dependence of K of the CoPtCr-SiO_2 media on the magnetic layer thickness.[31]

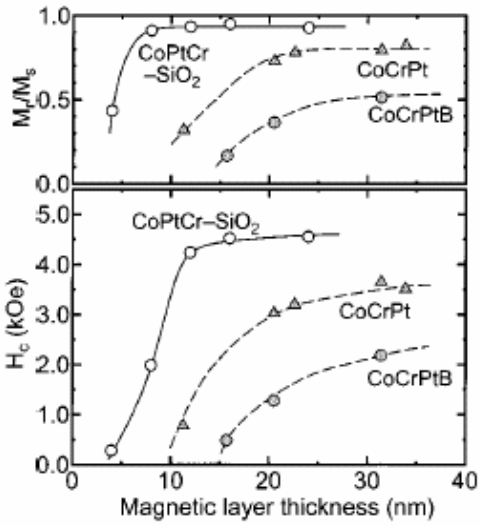

Figure 2.29 Dependence of Hc and Mr /Ms of the CoPtCr-SiO_2 media on the magnetic layer thickness.[31]

Fuji research center, T. Oikawa et al., firstly pronounced the significant granular media of CoPtCr-SiO_2 in 2002. The 12nm recording layer as shown in Fig. 2.28 and Fig. 2.29 illustrates a large perpendicular anisotropy of $4*10^6$ erg/ cm^3, and ultrahigh coercivity beyond 4 kOe, which are even larger than the conventional perpendicular media without oxide segregation such as CoCrPt and CoCrPtB.

Fig. 2.30 compares the roll-off curve of 12nm CoPtCr-SiO_2 media, with that of 30-nm-thick CoCrPtB media in terms of recording density. The CoPtCr-SiO_2 media could obtain much higher read-back signal than that of the CoCrPtB media, particularly in the ultrahigh-density recording more than 200 kfci. The recording resolution D_{50} of the CoPtCr-SiO_2 medium is about 320 kfci, which is about 1.4 times higher than that of the CoCrPtB. The high value D_{50} of the CoPtCr-SiO_2 media is likely to be result in the steep slope of the hysteresis loop, with very thin thickness of

the recording layer.

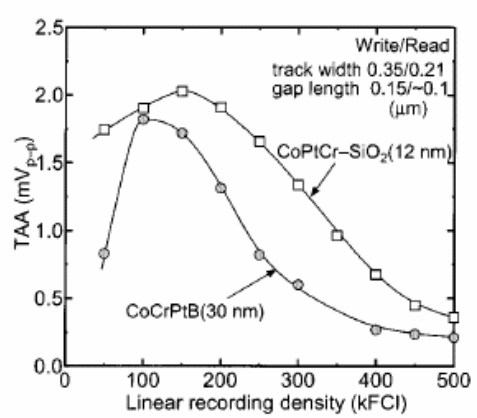

Figure 2.30 Roll-off curve of 12nm CoPtCr-SiO_2 media and 30nm CoCrPtB media [31].

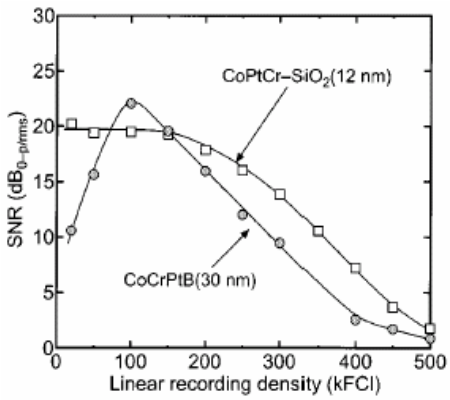

Figure 2.31 Recording density dependence of SNR of two different media [31].

Fig. 2.31 shows the recording density dependence on the signal-to-media-noise ratio (SNR) for these media. The SNR of the CoPtCr-SiO_2 media is about 5 dB greater than that of the CoCrPtB at 300 kfci. This is due to the well segregation of grain isolation structure of the CoPtCr-SiO_2 media shown in Fig. 2.24, which is very effective to improve SNR performance.

Moreover, worse loop squareness about 0.65 of the CoCrPtB media shows a large signal decay of 4.7%/decade and a small value ***Ku*** ($1.7*10^6$ erg/cm^3). On the other hand, there is almost no signal decay even in the 12nm CoPtCr-SiO_2 recording layer, which attributes to a large loop squareness and a large value ***Ku*** as mentioned just now.

In conclusion, the granular media shows better magnetic properties and high anisotropy ***Ku*** which are most suitable for ultra-high recording. Furthermore, the excellent SNR performance together with high thermal stability of CoPtCr-SiO_2 media may indicate that media possess the greater potential for high-density perpendicular recording media than the conventional one.

2.3 Recording Performance of Granular PMR

2.3.1 Origin of Media Noise form Layers

Recording Layer [4]

In 2000, K. Ouchi *et al.*, proposed a model of the noise source observed from MFM image of recorded pattern of single recording layer as described in Fig. 2.32. Through the formula expressed below, we could realize the relationship between the magnetic factors and the origin of noise.

$$\mathbf{En} \propto \mathbf{d} \bullet \mathbf{Ms} \bullet \delta^{3/2}(1\text{-}\mathbf{SQ})^{1/2}$$

En: medium noise amplitude **d**: reversed domain diameter

Ms: saturation magnetization **SQ**: perpendicular squareness

δ: media thickness

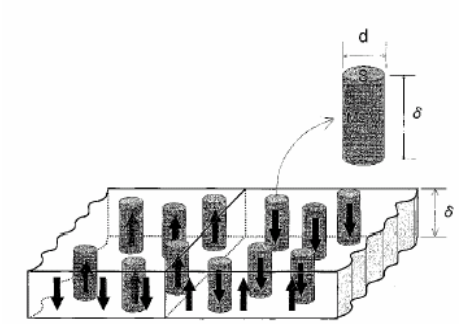

Figure 2.32 Noise source model for perpendicular recording media [4].

Reversed domain inevitable occurs to compromise the magnetostatic energy. Therefore, the media noise which is proportional to the domain size attributes to the reversed domains, while larger SQ would suppress the magnetostatic energy and subsequently the number of reversed domains. Consequently, large SQ and small domain size are vital for perpendicular media to enhance SNR performance. Moreover, thermal

stability and residual magnetization are also improved for the media with large SQ.

Soft Underlayer [32]

Although introducing soft underlayer would benefit a lot, an additional source of noise would occur on playback signal in the same time while the soft underlayer material was not properly optimized. The noise attributes to the domain walls in the soft underlayer; therefore, the best solution is to applying a biasing layer below soft underlayer.

Interaction between Recording layer & Soft Underlayer

There must be an interaction between hard magnetic material, i.e. CoPtCr-SiO_2 recording layer, and the soft magnetic underlayer due to magnetostatic energy. Consequently, the intermediate layers between recording layer and SUL are decisive introduced in order to decouple the interactions. However, the total thickness of intermediate layers can not be too high to lessen the magnetic flux back to the head as shown in Fig. 2.6.

2.3.2 Influence of Magnetic Cluster Size [33]

Magnetic cluster size calculated from a MFM image is useful to analyze the origin of media noise as shown in Fig. 2.33. However, the media noise and SNR improved as the size of magnetic cluster decreases. Therefore, the trade-off between the reduction of intergranular exchange

coupling and the prevention of thermal decay occur on reducing cluster size.

In addition, the perpendicular Hc is also enhanced as the trend while reducing the cluster size. It was clearly observed from Fig. 2.34 that the perpendicular Hc increases and magnetic cluster size reduced as decreasing the value of ($N_z - N_y$), which are calculated according to the magnetic cluster size assuming that the shapes of magnetic clusters are cylindrical. The relationship between perpendicular Hc and ($N_z - N_y$) can be understood by the formula in the right side of Fig. 2.44.

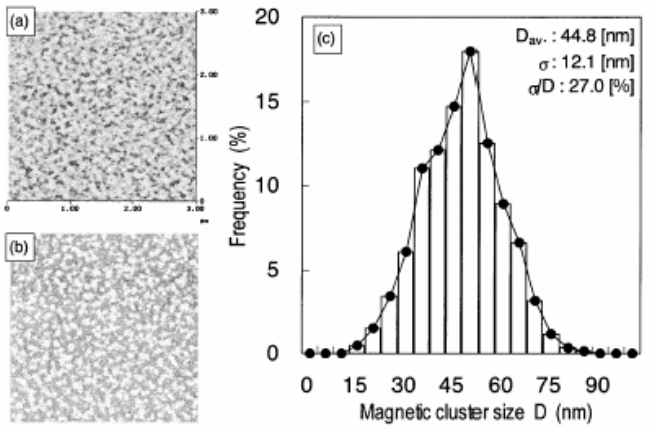

Figure 2.33 (a) Surface of a medium in the ac-erased state was observed. (b) Reversed domains were fitted using circles. (c) Circles were statistically totaled, and the average value of circles was defined as the magnetic cluster size [33].

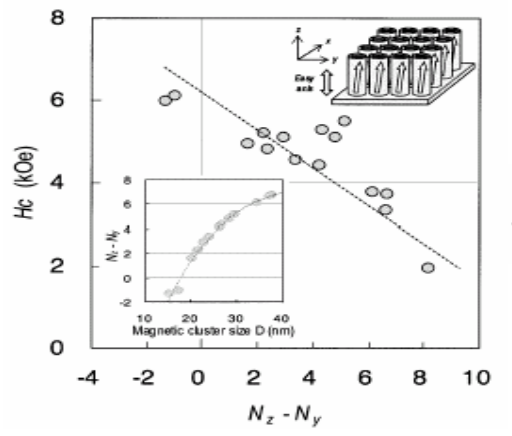

$$H_c = \frac{2K_u}{M_s} - (N_z - N_y)M_s$$

Figure 2.34 Hc dependence of 8 nm CoPtCr–SiO_2 media on the value of Nz-Ny . Nz and Ny are the z- and y-direction demagnetization factors, respectively [33].

As indicated in Fig. 2.35, noise increases and SNR decreases with increasing linear density, especially magnified at large magnetic cluster size. This represents that larger magnetic cluster sizes contribute to the main cause of increasing transition media noise as well as decreasing SNR performance. Moreover, for increasing bit density in order to achieve higher areal recording density, the effective method is to reduce the magnetic cluster size as illustrated in Fig. 2.36.

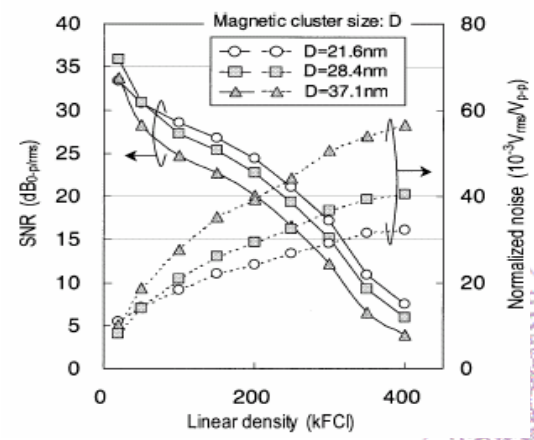

Figure 2.35 Recording density dependence of SNR and normalized media noise for various magnetic cluster sizes [33].

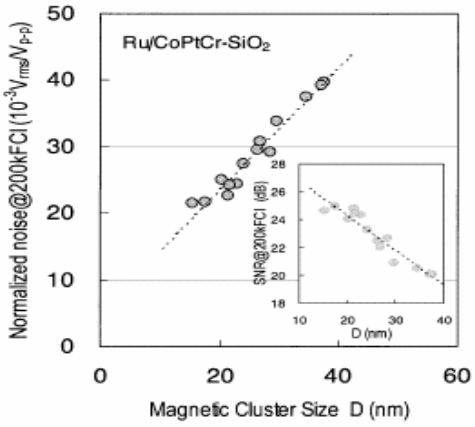

Figure 2.36 Magnetic cluster size dependence of normalized media noise and SNR at the recording density of 200 kfci [33].

2.3.3 Inter-granular Interactions

Since the issue of intergranular exchange coupling impacts the SNR performance of perpendicular recording media a lot, many studies had mentioned relevant factors to intergranular interactions. However, the real mechanism is too complicate to figure out conclusively and completely. Accordingly, it may need the computing assistant such as numerical simulation to realize the possible incidents.

2.3.3.1 Examining form Magnetic Loop [34] [35] [36]

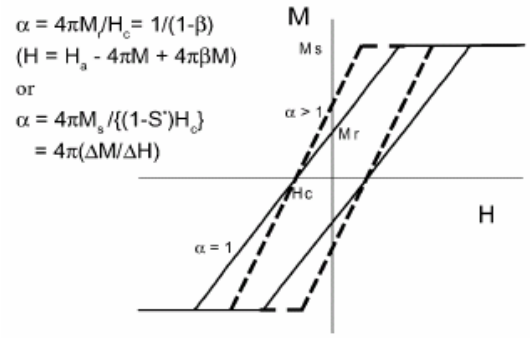

Figure 2.37 Loop slope parameter, α [34].

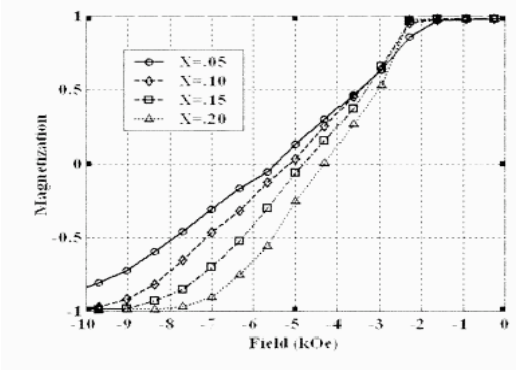

Figure 2.38 M-H loops as a function of exchange coupling field [35].

In general, the M-H loop slope α is introduced to realize inter-granular coupling as describes in Fig. 2.37. In addition, the curve of the media with large exchange coupling represents decreased perpendicular Hc and small negative Hn. Furthermore, large transition noise would occur on large amount of intergranular coupling especially at higher linear density. However, steeper M-H loop slope α, i.e. large exchange coupling and SQ, would reduce reversed domain effectively. As a result, the most important of all is to optimize the intergranular coupling to appropriate value; therefore, the SNR performance could be further promoted.

With resperct to magnetic cluster size ($D_{cluster}$), it usually increases as increasing the thickness of recording layer (δ), particularlly with little intergranular coupling. As seen from Fig. 2.39, the ratio of $D_{cluster}$ to δ is significant to the intergranular exchange coupling described as M-H loop slope α. α decreases as the value of $D_{cluster}$ / δ decreases, and reaches ～1 at Dcluster/ δ ～2. It implied that reduction of thickness of recording layer δ is necessary for small $D_{cluster}$ and appropriate α value.

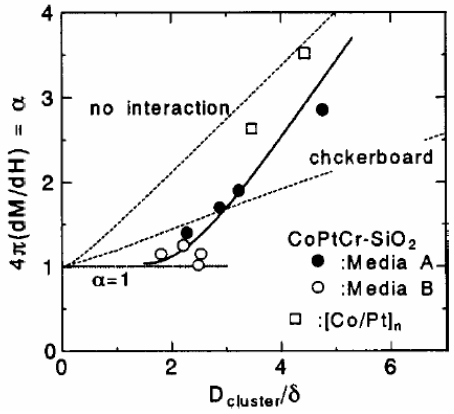

Figure 2.39 Loop slope parameter, α as a function of $D_{cluster} / \delta$ for the CoPrCr-SiO_2 media and $[Co/Pt]_n$ /NiAl superlattice media [36].

2.3.3.2 Remanence Coercivity [37] [38] [45]

From Sharrock's equation as described as fowllowing, Hr depends on

$$H_r(t') = H_0 \left[1 - \left\{ \frac{k_B T}{(K_u V_{\text{act}})} \ln \left(\frac{f_0 t'}{0.693} \right) \right\}^{1/2} \right]$$

the time scale in order to reverse the magnetization of grains, namely remanece coercivity. That is, the value of fixed field requred to reduce magnetization from saturation state to demagnetization state. For the sake of concerning the effect on thermal agitation of magnetization, Ho is used for intrinsic remanence coercivity obtained by subtracted the thermal effect as seen in Fig. 2.40, where H_k is anisotropy field calcuated as $2K_u/M_s$.

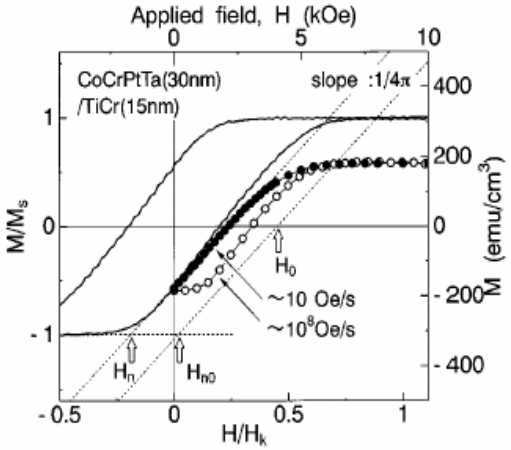

Figure 2.40 Typical remanence curves of CoCr based perpendicular media [45].

Fig. 2.41 represents that the value of H_o/H_k of different media increases as reducing the thickness of recording layer due to reduction of intergranular exchange coupling in the initail film growth. The clear obversation from numerical simulation result, as illustrates in Fig. 2.42, interprets that some grains have not switched, remain in the center of the bit cell while applying field. That is, the reversed domain seriously occurs on large value of H_o/H_k, i.e. weak intergranular exchange couling. Supposedly from simulation result, this effect attributes to the magneto-static interactions with already switched neighbors.

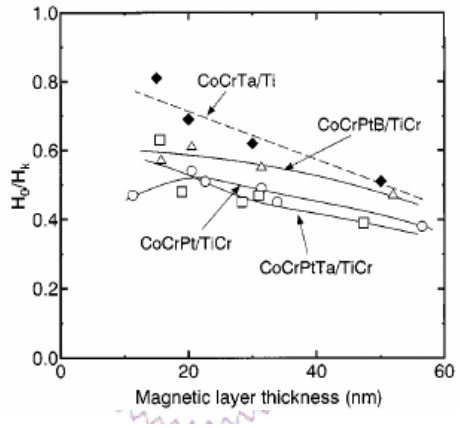

Figure 2.41 The dependence of H_o/H_k of the CoCrPt-(Ta, B) media on the magnetic layer thickness [38].

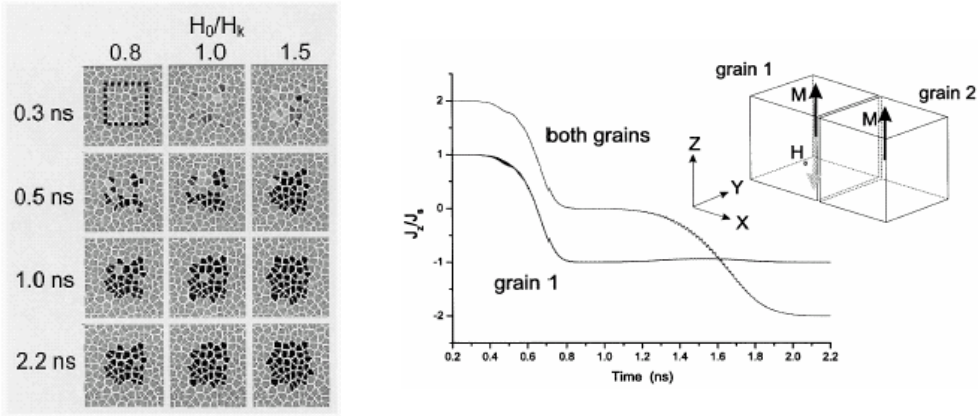

Figure 2.42 (left) Reversal of grains for different applied field (h = 0:05).The dashed line denotes the region where the external field is applied. Dark grey indicates reversed grains. (right) Time evolution of the z and x component (parallel and perpendicular to the field direction) of the magnetization [37].

2.3.3.3 ΔM measurement and Swithing Field Distribution(SFD)[39]

ΔM measurement is an effective method to identify intergranular coupling by calculated by DCD curve and IRM curve. The value of ΔM would determine the magnitude of interactions. On the other hand, swithing field distribution (SFD) would give the imformation about the dispersion of the fiels required to switch the magnetic cluster, which is important for recording performance especailly for ultra-high recording density. Large switching would direct impacts the resolution of recording bits and recording density, while small switching field would easier swiching the magnetization of the grains and therefore the achievable maintenanece lifetime. The detail calculations of ΔM measurement and SFD are mentained as following.

IRM Remanence Curve and DCD Remanence Curve [40] [41]

In a DCD measurement as shown in Fig. 2.43 (a), the film is initially negatively magnetized firstly and then the remanent magnetization, i.e. magnetization at zero field, is subsequently measured as a function of increasing positive applied field. An IRM measurement also measure the remanent magnetization versus increasing applied field. However, the initial state for the IRM measurement is an ac demagnetized state, i.e. zero magnetization, instead of a fully magnetized state, as seen in Fig. 2.44 (a).

ΔM is considered about the Stoner-Wohlfarth relation for non-interacting single domain particle , which is only suitable for ideal grian model and calculated from DCD curve and IRM curve as follows:

$$M_{\mathrm{DCD}}(H) = 1 - 2M_{\mathrm{IRM}}(H)$$

In fact, there is some deviation between real case and ideal model, and subquently the relation is redefined as follws:

$$\Delta M(H) = M_{\mathrm{DCD}}(H) - [1 - 2M_{\mathrm{IRM}}(H)]$$

For both calculation SFD and ΔM, the remanence curves have to be expressed according to the actual field (H_{total}) acting on grains instead of external field (H_{ext}) as following equation, where N is effective demagnetion factor valued between 0 and 1. The correction is concerning that H_{total} includes demagnetization contribution which would leads to broadening of DCD curve and IRM curve in addition to ΔM measurement and SFD.

$$H_{\mathrm{tot}} = H_{\mathrm{ext}} - 4\pi NM \qquad 0 \leq N \leq 1$$

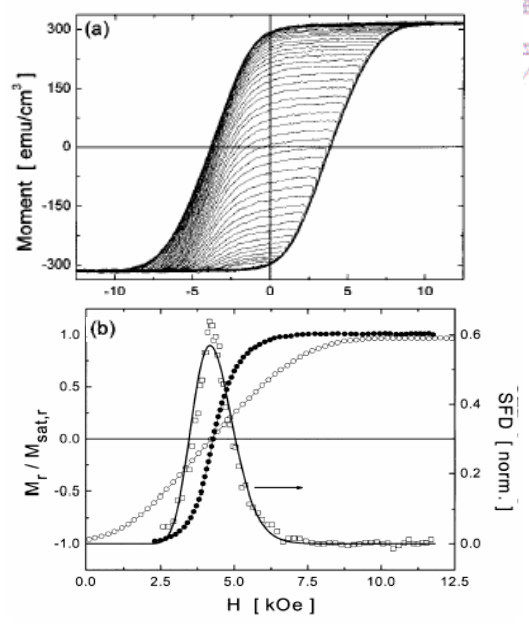

Figure 2.43 (a) DCD recoil loops (b) DCD curve with and without correction as well as SFD. The solid line is fitting as the log-normal distribution [41].

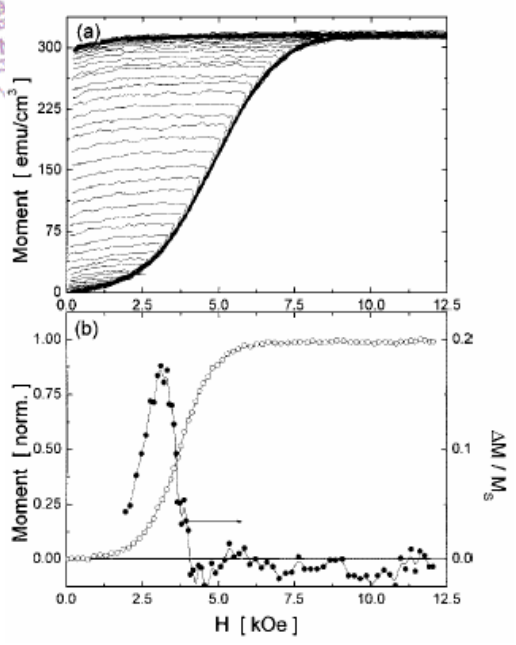

Figure 2.44 (a) IRM recoil loops (b) IRM curve and ΔM curve after demagnetization correction [39].

Subsequently, the correction of DCD curve and IRM curve are described as open circles in Fig. 2.43(b) and Fig. 2.44(b), respectively. In addition, the appearence of ΔM is illustrated as solid cirles in Fig. 2.44(b). On the other hand, the switching field distribution is defined as the differentiated DCD remanence curve by H_{total} as open circles which is fitting as the log-normal distribution in Fig. 2.44(b), i.e. d M_{DCD} / d H_{total}.

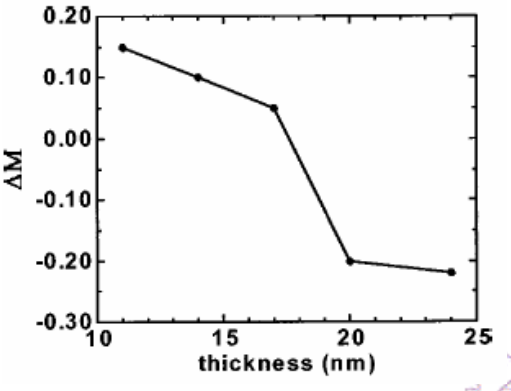

Figure 2.45 Thickness dependence of the ΔM for the CoCrPt alloy [40].

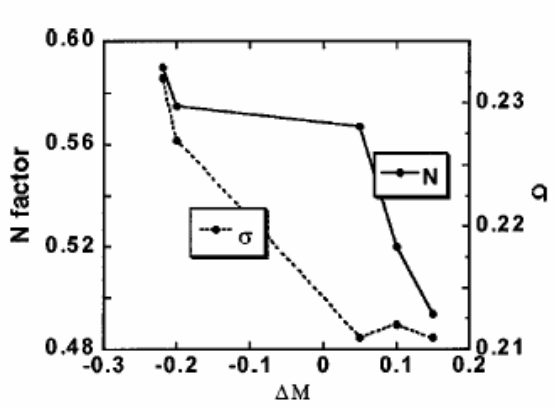

Figure 2.46 ΔM dependence of the effective N (solid line) and the SFD (dashed line) [40].

From Fig. 2.45, ΔM (H) changes from positive to negative, indicating a reduction of the exchange interaction in thicker films which is due to strong interactions in the initial state of film growth. Fig. 2.46 indicates that ΔM greatly depends on both effective N and standard deviation of SFD. While increasing the exchange coupling, ΔM changes from negative to positive. In the meantime, the effective N drops from 0.59 to 0.50 and the standard deviation of SFD decreases from 0.24 to 0.21.

In conclusion, using the measurement of ΔM and SFD would not only realize the intergranular exchange coupling but improve the recording performance such as media noise. These modern analyses will be more and more impressed in the future.